Final Draft
of the original manuscript:

Boschetti de Fierro, A.; Lorenzo, A.T.; Mueller, A.J.; Schmalz, H.; Abetz, V.:
Crystallization Kinetics of PEO and PE in Different Triblock Terpolymers: Effect of Microdomain Geometry and Confinement
In: Macromolecular Chemistry and Physics (2007) Wiley

DOI: 10.1002/macp.200700434

Title page

Crystallization Kinetics of PEO and PE in Different Triblock Terpolymers: Effect of Microdomain Geometry and Confinement

Adriana Boschetti-de-Fierro, Arnaldo T. Lorenzo, Alejandro J. Müller, Holger Schmalz, Volker Abetz*

A. Boschetti-de-Fierro, V. Abetz

Institute of Polymer Research, GKSS Research Centre Geesthacht GmbH, 21502 Geesthacht, Germany. Fax: (+49) 4152 872446. E-mail: volker.abetz@gkss.de

A. T. Lorenzo, A. J. Müller

Grupo de Polímeros USB, Departamento de Ciencia de los Materiales, Universidad Simón Bolívar, Apartado 89000, Caracas 1080-A, Venezuela

Holger Schmalz

Makromolekulare Chemie II, Universität Bayreuth, 95440 Bayreuth, Germany

Keywords:

block copolymers, crystallization, differential scanning calorimetry (DSC), morphology.

Abstract:

Isothermal crystallization kinetics of poly(ethylene oxide) (PEO) and polyethylene (PE) blocks within various triblock terpolymers was studied by differential scanning calorimetry (DSC). The effect of the geometry of the microdomains was analyzed by studying different compositions of polyethylene-*block*-polystyrene-*block*-poly(ethylene oxide) (PE-*b*-PS-*b*-PEO) triblock terpolymers. It was found that the crystallization rate decreases when the block content decreases for both crystallizable blocks. The effect of the microdomain geometry, confinement or chain tethering on the crystallization of PEO was extensively studied by comparing pairs of triblock terpolymers with differences either in the nature (crystalline, glassy, amorphous) or in the location of the other blocks in the terpolymer (end block, middle block, i.e., PE-*b*-PS-*b*-PEO, PS-*b*-PE-*b*-PEO). It was found that the PE block can nucleate the PEO block, nevertheless, it reduces the segmental mobility of its neighboring blocks. A rubbery neighbor block makes crystallization slower than a glassy one. Crystallization proceeds slower in the middle block than in the end block. For the PE block we found that the crystallization rate decreases more strongly with increasing geometrical confinement than by locating the block as a middle block instead of an end block.

Text pages

Introduction

Semi-crystalline block copolymers are materials that attract great interest due to their tailored mechanical properties and various possible morphologies.[1-9] The morphology is determined by a competition between two factors:[9-14] the block copolymer self-assembly ability,[15] which is based on the interaction among the different blocks and organizes the incompatible blocks into separated microphases, and the crystallization of the crystallizable block(s). The final morphology has been found to be path-dependent, based on whether the crystallization occurs from a homogeneous state or a microphase-separated one.[14, 16]

In general, the resultant morphology can be categorized as follows: [2-5, 11-13, 17] (a) microphase separation is driven by crystallization when $T_c > T_{ODT} > T_g$, and a lamellar morphology would be created; (b) a lamellar morphology is the result in weakly segregated systems with soft confinement ($T_{ODT} > T_c > T_g$); and (c) in strongly segregated systems with hard confinement, i.e., $T_{ODT} > T_g > T_c$, the preformed morphology is retained and confined morphologies are formed, such as spheres, cylinders or lamellae.

There has always been interest in the study of polymer crystallization due to the mechanical properties of crystallizable polymers. The crystallization process is, however, far from being well understood, and many discussions have taken place during the last decade.[18] The study of crystallization within block copolymer microphases is advantageous mainly for the possibility of adjusting the nucleation process due to the confined crystallization in nanoscopic dimensions.

In this work the crystallization kinetics of polyethylene (PE) and poly(ethylene oxide) (PEO) as constituent blocks in different triblock terpolymers is studied. The effect of composition, which causes the generation of different morphologies, i.e., confinements on the

crystallizable block, on crystallization will be investigated. Various confinement types were investigated using a wide diversity of triblock terpolymers and topologies. The effects of glassy, rubbery and semi-crystalline blocks as middle blocks or end blocks on the crystallization of the PEO end block are investigated. The influence of the chain topology will also be addressed as the kinetics is calculated on the PE middle block.

Experimental Part

Synthesis. Anionic polymerization was carried out using solvents and monomers purified according to common procedures described elsewhere.[6, 19] The synthesis of poly(1,4-butadiene)-*block*-polystyrene-*block*-poly(ethylene oxide) (PB-*b*-PS-*b*-PEO) triblock terpolymers was realized by sequential anionic polymerization of butadiene, styrene, and ethylene oxide in benzene with *sec*-BuLi as initiator. Polymerization of ethylene oxide in the presence of a lithium counterion was accomplished by using the strong phosphazene base *t*-BuP_4.[2, 20] The same procedure was used to synthesize polystyrene-*block*-poly(1,4-butadiene)-*block*-poly(ethylene oxide) (PS-*b*-PB-*b*-PEO) triblock terpolymers. The polymerization of butadiene under the conditions employed led to a preferential 1,4-addition (Table 1), which is essential to get the corresponding "pseudo polyethylene" structure after hydrogenation.

The hydrogenation of the PB-*b*-PS-*b*-PEO triblock terpolymers (precursor) resulted in the corresponding PE-*b*-PS-*b*-PEO triblock terpolymers. Homogeneous catalytic hydrogenation was carried out with Wilkinson catalyst $(Ph_3P)_3Rh(I)Cl$. Further purification in order to eliminate residual Wilkinson catalyst was performed. In the terpolymer notation employed here ($A_xB_yC_z^m$), the subscripts denote the mass fraction in percent and the superscript indicates the overall number-average molecular weight M_n of the block copolymer in kg/mol.

(Insert Table 1)

Differential Scanning Calorimetry (DSC). A Perkin-Elmer PYRIS 1 differential scanning calorimeter in a dry nitrogen atmosphere with a CCA 7 liquid nitrogen cooling device was used. For all measurements a two-point calibration with *n*-decane and indium was applied. Samples of 8.0 ± 0.5 mg were placed in the DSC pans. Standard and isothermal scans, as well as self-nucleation experiments were performed.

Isothermal Scans. Two different thermal protocols were employed in order to record the isothermal crystallization of PE in the hydrogenated samples or of PEO blocks either in the non-hydrogenated or in the hydrogenated terpolymers. Prior to the isothermal scans the crystallization temperature T_c was determined in order to ensure that crystallization does not occur during the cooling scan.

Isothermal crystallization of the PE block, and PEO block in non-hydrogenated terpolymers: samples were heated up to 120 °C and held at that temperature for 3 min in order to erase thermal history. Then they were quenched down to T_c at 80 °C/min, and the isothermal crystallization was followed.

Isothermal crystallization of the PEO block in hydrogenated terpolymers: samples were also heated up to 120 °C and held at that temperature for 3 min in order to erase thermal history, followed by a cooling scan to –100 °C at 10 °C/min, in order to induce crystallization in both PE and PEO blocks. Subsequently, a heating scan was performed at 10 °C/min up to 70 °C, and a 75 min isotherm was realized in order to melt completely the PEO block and reach saturation levels of PE crystallization. These conditions were chosen to assure that all PEO crystals are molten and PE has crystallized to a degree where no further crystallization occurs during the following step. Finally, the sample was cooled down to T_c at 80 °C/min, and the isothermal crystallization was recorded.

Step crystallization: if the crystallization enthalpy is very low, the signal to noise ratio might be too low and the results have high associated errors. In that case, the isothermal crystallization was followed by steps.[7, 21] In the same afore-mentioned way, samples were heated up to 120 °C and held at that temperature for 3 min in order to erase thermal history. Then, they were quenched down to T_c at 80 °C/min, and the isothermal crystallization was followed during a given time t_c. Finally, the sample was heated from T_c up to 120 °C and the melting enthalpy was determined. The process was repeated for crystallization times varying from 0.1 min to 300 min, until a saturation in the melting enthalpy was reached. The saturation enthalpy was assigned to 100% relative crystallinity, and the degree of crystallinity was calculated for each crystallization time.

Self-Nucleation (SN) Experiments. Self-nucleation measurements were performed in analogy to the procedure described by Fillon et al.[22] The complete thermal treatment has been explained in detail elsewhere.[3, 13] The protocol used can be summarized as follows: 1) Melting of the sample at 120 °C during 5 min in order to erase any previous thermal history. 2) Subsequent cooling at a rate of 10 °C/min to -100 °C, which creates a ‘‘standard’’ thermal history. 3) Partial melting by heating at 10 °C/min up to a ‘‘self-nucleation temperature’’ T_s. 4) Thermal conditioning at T_s for 5 min. Depending on T_s, the crystalline PE or PEO domains will be completely molten, only self-nucleated, or self-nucleated and annealed. If T_s is sufficiently high, no self-nuclei or crystal fragments can remain, and the sample is then in so-called Domain I, the complete melting domain. At intermediate T_s values, the sample is almost completely molten, but some small crystal fragments or crystal memory effects remain, which can act as self-nuclei during a subsequent cooling from T_s, and the sample is said to be in Domain II, the self-nucleation domain. Finally, if T_s is too low, the crystals will be only partially molten, and the remaining crystals will undergo annealing during the 5 min at T_s, while the molten crystals will be self-nucleated during the later cooling, and the sample is in Domain III, the self-nucleation and annealing domain. 5) Cooling scan from T_s at 10

°C/min, where the effects of the previous thermal treatment will be reflected on crystallization. 6) Heating scan at 10 °C/min to 120 °C, where the effects of the thermal history will be apparent on the melting signal.

Results and Discussion

The triblock terpolymer thermal properties were determined by standard DSC scans, as already presented elsewhere.[23] It was found that the mentioned properties depend on the molecular weight of the blocks, and more interestingly on the morphology. That effect is investigated now based on the crystallization kinetics of each crystallizable block. The variety of triblock terpolymers synthesized allows us to carry out a discussion based on different parameters, such as the overall morphology, physical properties of the end block and the middle block and sequence of the blocks in the terpolymer.

Crystallization kinetics of the PEO block. Crystallization kinetics was studied by recording the isothermal crystallization of the samples quenched from the molten state to the given crystallization temperature. An example of the isothermal crystallization scans that corresponds to $B_{29}S_{40}EO_{31}{}^{168}$ at different temperatures is presented in Figure 1a.

(Insert Figure 1)

The enthalpy of crystallization was calculated as a function of time via integration of the isothermal scans. The relative crystallinity was calculated considering the enthalpy of crystallization was 100% when the crystallization exotherm displays a constant value and has returned to the baseline. This treatment can lead to crystallization values higher than 100 % due to baseline oscillations towards the end of the crystallization process, which have no physical meaning and do not affect further calculations in the low crystallinity range. In Figure 1b a representation of the relative crystallinity is presented as a function of the crystallization time for $B_{29}S_{40}EO_{31}{}^{168}$.

In the cases where the crystallinity curves presented the typical sigmoidal shape as in Figure 1b, the data of the initial stages of crystallization (i.e., for relative degrees of crystallinity between 5 and 35%) was fitted to the Avrami equation:[24-26]

$$1 - V_c(t) = \exp(-kt^n) \quad (1)$$

where V_c is the relative volumetric transformed fraction (from molten to crystalline state), k is an overall crystallization rate constant for nucleation and growth, and n is the constant known as Avrami index. In the Avrami theory, the Avrami index is an integer number between 1 and 4 which value is considered to consist of two contributions.[7] The first one is related to the nucleation (instantaneous = 0, sporadic = 1), and the second one is related to the dimensionality of the crystal or superstructure (line = 1, disc = 2, sphere = 3). There have been many discussions regarding the limitations in the use of the simplified Avrami equation and its variables, especially in the case of crystallizable block copolymers.[27] The theory was developed for the crystallization of molecules, and there are certain assumptions and simplifications such as the homogeneous nuclei distribution and radial crystalline growth.[25] An extended equation was also developed based on heterogeneities as nuclei and an extended volume term,[26] which is applicable to the case of confined polymer crystallization.

The simplified version of the Avrami equation has been widely used in the literature as one possible fitting routine for crystallization kinetics data in crystalline block copolymers.[12, 28-32] If the crystallization curve of the crystallizable block shows a sigmoidal dependence of the crystallinity with time, then the kinetics is usually well represented by Avrami indices varying in the range between 2 and 4, as typically found for homopolymers.[31] The crystallinity data is always fitted in the range of primary crystallization (considered to be approx. below 40% of relative crystallinity).

The particular case of confined crystallization inside a nanophase and its analysis by means of the Avrami equation have been very much discussed in the literature.[27, 33] It was observed by Loo et al.[12, 34] that the relative crystallinity curve of a chemically confined system was not sigmoidal but exponential, which means that it followed a first-order kinetics. Due to the restrictions in scale, it is assumed that the rate-determining step in confined crystallization is the nucleation. Once a nucleus is formed, the crystalline growth can be referred to as instantaneous, and the crystallization is complete before a second nucleus is formed.[34] Therefore, the crystallinity can be described as:[11, 30, 35]

$$a_c(t) = 1 - \exp(-kt) \tag{2}$$

which is an expression developed by considering the nucleation as the rate-determining step,[35] and describes an exponential function instead of a sigmoidal one. In Equation (2), the term a_c(t) is the fraction of transformed material from the molten to the crystalline state. It must be stressed that Equation (2) is equivalent to the Avrami equation (Equation (1)) with $n = 1$.[34] The assumption of randomness of nuclei generation made during the development of the simplified Avrami equation might be considered to be violated in the case of confined crystallization. Equation (2) is generated considering the crystallization in droplets or dispersed domains (see the work of Turnbull and Cormia in ref. **Fehler! Verweisquelle konnte nicht gefunden werden.**, as well as the contributions from Loo and Register cited in ref. 11 and 34). The equivalence of the two expressions despite the differences in starting considerations might appear striking, but it is not the matter of this contribution.

The Avrami equation has the advantage that it can describe kinetics from order 0 to 4 with a simple equation and only two adjustable parameters. Even though it can only fit data up to 50% relative crystallinity in the majority of cases, its use is well accepted because there is no alternative theory available that is as elegant as this. All the modifications that have been

made in order to improve it have just added more fitting parameters, which generates more ambiguous fittings.

The crystallization kinetics can also be analyzed by means of the crystallization rate. A convenient parameter to represent the crystallization rate is $1/\tau_{50\%}$, where $\tau_{50\%}$ is the experimentally determined half-crystallization time, i.e., the time at which the crystallization degree is half of the total relative crystallization. In this contribution, this parameter has been experimentally determined for the different experiments, and is plotted as a function of the crystallization temperature employed for each material.

The morphologies have been determined by small-angle X-Ray scattering (SAXS), transmission electron microscopy (TEM) and scanning force microscopy (SFM) as presented elsewhere.[23, 36] For the mentioned compositions, morphologies composed of PEO spheres in a polystyrene matrix, cylinders in a polystyrene matrix and lamellae were found, respectively. An overview of the found morphologies is presented in Table 2.

(Insert Table 2)

(Insert Figure 2)

The crystallization kinetics of the poly(ethylene oxide) block has been studied in different triblock terpolymers. Figure 2a shows the relative crystallinity as a function of the crystallization time for a crystallization temperature of 48.0 °C for $B_{29}S_{40}EO_{31}^{168}$ and $B_{37}S_{16}EO_{47}^{76}$, while Figure 2b presents the values of $1/\tau_{50\%}$ as a function of the crystallization temperature for $B_{16}S_{68}EO_{16}^{210}$, $B_{29}S_{40}EO_{31}^{168}$ and $B_{37}S_{16}EO_{47}^{76}$, three triblock terpolymers with different compositions and different morphologies. The crystallization of the PEO block in $B_{16}S_{68}EO_{16}^{210}$ was not possible at 48.0 °C, and therefore the values at 40 °C are presented. The presented curves for $B_{37}S_{16}EO_{47}^{76}$ and $B_{29}S_{40}EO_{31}^{168}$ show the typical sigmoidal shape

properly described by the Avrami equation with Avrami indices of 2.5-3.5 (Figure 2a). This indicates that crystallization mechanism in the lamellar ($B_{37}S_{16}EO_{47}^{76}$) and cylindrical ($B_{29}S_{40}EO_{31}^{168}$) arrangements is essentially identical to the conventional spherulitic, long-range crystal growth from the heterogeneous nuclei. The similarity between the behavior of the lamellar and cylindrical morphology is expected due to defects in the morphology that allow interconnection of the microphases.

The curve presented for $B_{16}S_{68}EO_{16}^{210}$ is exponential, which corresponds to first-order crystallization kinetics and implies that the crystallization of the PEO block is taking place inside the isolated microdomains.[34] The low crystallization temperatures also indicate that the crystallization of the PEO block is taking place exclusively in confined microdomains, as was discussed in our previous work.[23] Self-nucleation experiments were carried out on this sample in order to confirm the confinement of the crystallization, and are presented and discussed further in this contribution.

From the results in Figure 2b one can see that the crystallization rate for a given crystallization temperature is higher for $B_{29}S_{40}EO_{31}^{168}$ compared to that of $B_{37}S_{16}EO_{47}^{76}$, but both show a much higher rate than obtained for $B_{16}S_{68}EO_{16}^{210}$. This tendency indicates that the crystallization rate decreases when the block content decreases significantly. The higher crystallization rate observed for $B_{29}S_{40}EO_{31}^{168}$ can also be a consequence of highly interconnected cylinders, and the effect of the morphology (i.e., the effect of the block content) can only be clearly appreciated when the domains are isolated. It should also be noted that the decrease in block content represents in these cases not only a decrease in size of the domains. It also implies an increase in the interfacial area (from sheets or cylinders to spheres). The propagated errors associated to the crystallization half-times have been included in Figure 2b, and it is evident that they are extremely small for those experiments carried out via isothermal crystallization. They are more notable for the values calculated

from step crystallization experiments, but are still significantly smaller than the observed variation in $\tau_{50\%}$.

The previous results establish the effect of the microdomain geometry on the crystallization kinetics. In the following, the effect of the structure of the neighboring blocks will be analyzed. The first of three cases is related to the effect of having a crystallizable block instead of an amorphous block at the other end of the chain. This will be illustrated by comparing $B_{29}S_{40}EO_{31}^{168}$ and $E_{29}S_{40}EO_{31}^{170}$, which are triblock terpolymers forming PEO cylinders before and after hydrogenation.

(Insert Figure 3)

The crystallization describes a sigmoidal shape as a function of time for the two triblock terpolymers presented in Figure 3a, which differ in the nature of the end block opposite to the PEO block. The fitting to the Avrami equation gave values of Avrami indices of 2.5 – 3.0, consistent with the conventional crystallization mechanism already mentioned. The crystallization rate (Figure 3b) is lower for the non-hydrogenated terpolymer than for the hydrogenated, i.e., the crystallization of the PEO block is faster in $E_{29}S_{40}EO_{31}^{170}$. The onset of crystallization takes place earlier, which could indicate an increase in the nucleation rate. This behavior was observed for all triblock terpolymer pairs, independent from composition and morphology.

If the PE crystals nucleate the PEO chains, then the information is somehow transmitted through the PS domains. This fact may be possible due to local sub-T_g flow processes at temperatures close to T_g. The increase in local density caused by crystallization generates either voids between the microphases[37] or causes local flow in order to endure volume constriction. Since voids were not observed in the bulk samples, a local flow of the glassy PS chains is assumed. Thus, PE crystallization would lead to a reduction of PS at the interface

with PEO, and as a result the PEO chains undergo a significant stretching at the PS/PEO interface. If this local stretching can assist nucleation for crystallization, then the crystallization can take place without overcoming the activation energy barrier of nucleation. This will result in a facilitated crystallization of PEO from that interface, with higher a crystallization rate. A similar nucleation mechanism has been proposed for the crystallization in a liquid phase-separated blend, where the concentration fluctuations caused by spinodal decomposition during phase separation were found to generate crossover and facilitate the nucleation for crystallization.[38]

The second case related to the effect of the physical nature of the surrounding blocks on the crystallization kinetics of the PEO block is illustrated by comparing $E_{16}S_{40}EO_{44}$[144] with $S_{43}E_{22}EO_{35}$[112], as shown in Figure 4. By altering the triblock terpolymer block sequence of the hydrogenated terpolymers, the effect of the PEO chain anchored to the PE semicrystalline phase is investigated. Again, the relative crystallinity (Figure 4a) described a sigmoidal curve, and the calculated Avrami indices are 1.8 – 2.5. These values are lower than the ones expected for homopolymers and presented here to this point. Similar results have been reported in the literature in cases where the crystallization occurs under confinement without any change in the crystallization mechanism, i.e., heterogeneous nucleation under confinement reflects typical values of Avrami indices below 2.[11, 31]

(Insert Figure 4)

According to the results presented in Figure 4b, slightly lower crystallization rates were found for $S_{43}E_{22}EO_{35}$[112], where the PE block is next to the PEO crystallizable chain. In the terpolymers compared in this case, the PE block is a semicrystalline phase with a crystallinity degree around 30%. Therefore, the crystallizable PEO phase is likely surrounded by a rubbery, amorphous PE phase, and this decreases the crystallization rate of the PEO block.

The effect of a rubbery neighbor block will be further analyzed with the following example.

The third and last case of the environment effect on crystallization of PEO considers the classic soft-hard confinement effect. Two comparisons will be described. First, a comparison between $E_{16}S_{40}EO_{44}$[144] and $E_{19}EP_{40}EO_{41}$[138] is depicted in Figure 5. The $E_{19}EP_{40}EO_{41}$[138] is a polyethylene-*block*-poly(ethylene-*alt*-propylene)-*block*-poly(ethylene oxide) triblock terpolymer obtained from the catalytic hydrogenation of poly(1,4-butadiene)-*block*-poly(1,4-isoprene)-*block*-poly(ethylene oxide), synthesized by sequential anionic polymerization.[39] In both cases the morphology consists of PEO cylinders in either a PS or a PEP matrix, while the PE crystals are distributed in the matrix as axialites, as reported elsewhere.[23, 39]

(Insert Figure 5)

The sigmoidal crystallization curves presented in Figure 5a were fitted with the Avrami equation and returned values of Avrami indices of 1.8 – 2.5 for $E_{16}S_{40}EO_{44}$[143] and 2.5 – 3.0 for $E_{19}EP_{40}EO_{41}$[138]. The latter corresponds to the crystallization mechanism common to homopolymers, while the case of $E_{16}S_{40}EO_{44}$[143] has been discussed in the preceding section. In view of the similarities in composition and the differences in confinement, it could be speculated that a rubbery matrix causes less confinement than the glassy one.

The crystallization rate shown in Figure 5b is lower for the PEO in the terpolymer with a rubbery PEP middle block. Consequently, the crystallization of PEO is slowed down due to the high mobility of the rubbery middle block, as was also assumed in Figure 4b. The high mobility results in a restriction for the crystallization of PEO from that interface. In related works, the crystallization kinetics of poly(*p*-dioxanone)-*block*-poly(*ε*-caprolactone) diblock copolymers were investigated and in the temperature range where the poly(*ε*-caprolactone) block was molten, the isothermal crystallization kinetics of the poly(*p*-dioxanone) block was greatly depressed as compared to that of an equivalent homopolymer since the topological

restrictions imposed by the highly mobile covalently bonded poly(ε-caprolactone) chains increase the energy barrier for secondary nucleation.[8, 29, 40] Similar results where the crystallization rate of a crystallizable block is slowed down by a covalently bound rubbery neighbor block have been reported by Ueda et al.[41] and by Shiomi et al.[32]

The relative crystallinity as a function of time is shown in Figure 6a for $B_{16}S_{40}EO_{44}$[143] and $S_{43}B_{21}EO_{36}$[111] at the indicated crystallization temperatures. Here, the block sequence of the non-hydrogenated triblock terpolymer was altered, i.e., the glassy PS neighbor is substituted by a rubbery PB block. Since it was not possible to achieve the crystallization of the PEO block in the two triblock terpolymers at the same crystallization temperature range, the crystallization curves are presented only to confirm their sigmoidal shape, but no further conclusions can be drawn from this. In addition, the crystallization rate, indicated by the inverse of crystallization half time in Figure 6b, is lower when the PB is located in the middle block position compared to PB as an end block. This behavior is due to the same effect mentioned for $E_{19}EP_{40}EO_{41}$[138], since the high mobility of the neighbor block slows down the incorporation of the free chain segments to the growing nuclei and therefore decreases the crystallization rate.

(Insert Figure 6)

The effect of the block sequence in the crystallization of the PEO end-block has been studied by Epps et al. in polystyrene-*block*-polyisoprene-*block*-poly(ethylene oxide) (SIEO) and polyisoprene-*block*-polystyrene-*block*-poly(ethylene oxide) (ISEO).[42] They have found that the melting temperatures of the PEO block within the ISEO samples, at a given domain size, were all significantly lower than those for the SIEO counterparts. It was concluded that this melting point reduction effect is attributable to hard vs. soft wall confinement, since the glassy PS domains could offer more effective confinement than rubbery PI domains, thereby better suppressing crystallization. This effect is in good agreement with the difference in

melting temperatures between $B_{16}S_{40}EO_{44}$[143] and $S_{43}B_{21}EO_{36}$[111] (T_m = 61.4 and 62.9 °C, respectively). The melting point depression in the case of $E_{16}S_{40}EO_{44}$[143] and $E_{19}EP_{40}EO_{41}$[138] is also following the same tendency, although the difference could also be regarded as negligible (T_m = 63.6 and 63.8 °C, respectively). Here we observed differences between the confinement and the crystallization rate. The glassy PS block is a hard wall confinement and suppresses the crystallization, but that does not imply that the crystallization rate is lower than in the soft wall confinement conditions.

It is interesting that in both Figures 5 and 6 the rubbery block (PEP and PB respectively) has a higher effect on the crystallization rate of the PEO block than a neighboring glassy block like PS. This trend may depend on the difference between the crystallization temperature and the T_g of the rubbery block, since reverse trends have been recently observed in different systems. Müller et al.[43] have recently investigated the crystallization of the PE block within diblock copolymers containing different neighboring blocks. A glassy block of polystyrene (PS), a rubbery block of poly (*D,L*-lactide) (PDLA), a semicrystalline block of poly (*L*-lactide) (PLLA) and a miscible block of poly(ethylene-*alt*-propylene) (PEP) were used to asses the influence of the degree of confinement and miscibility on the crystallization kinetics of PE. PEP had the largest effect on the crystallization kinetics of the PE block in view of its miscibility with molten PE. For the strongly segregated systems larger restrictions were imposed by vitreous PS due to hard confinement as compared with the soft confinement of the rubbery PDLA block. A nucleation effect of previously crystallized PLLA on the PE block was detected which offsets its depression of the crystallization kinetics of PE. Since the T_g of PDLA is 55 °C and the crystallization temperatures for the PE block employed were only 30 to 40 °C above this value, the mobility of the PDLA chains may not be as large as those of PB (T_g = -101 °C) and PEP (T_g = -57 °C) at these temperatures.

Crystallization kinetics of the PE block. The crystallization kinetics of the PE block was also investigated. The effect of the morphology as well as the position of the crystallizable block,,i.e., middle or end block resulting in differences in chain tethering, is presented in Figure 7. The morphology effect on crystallization kinetics of PE has also been studied on diblock copolymer systems, and is reported in a different contribution.[44] The development of relative crystallinity with crystallization time is presented in Figure 7a. While the crystallization was followed at 73.0 °C for $E_{29}S_{40}EO_{31}^{170}$ and $S_{43}E_{22}EO_{35}^{112}$, the range of crystallization temperature obtained for $E_{38}S_{16}EO_{46}^{77}$ was much higher and therefore the crystallization curve is presented at a different temperature, i.e., 80.0 °C.

The crystallization curves in Figure 7a for $E_{29}S_{40}EO_{31}^{170}$ and $E_{38}S_{16}EO_{46}^{77}$ show the typical sigmoidal shape, with Avrami indices of 1.5 – 2.0 and 2.0 – 2.5, respectively. The shape of the curves and the indices above 2 indicate that the crystallization mechanism is similar to the conventional spherulitic one, including long-range crystal growth from the heterogeneous nuclei. As was mentioned before, indices below 2 are assumed to be a consequence of confinement, while the crystallization mechanism is assumed to remain unchanged.[11, 31] The crystallization curve of $S_{43}E_{22}EO_{35}^{112}$ shows an exponential dependence (Figure 7a). This behavior is described as a first order crystallization kinetics, and it is attributed to crystallization into a confined microphase, where the nucleation is the rate-determining step of the crystallization process.[34] Therefore one can conclude that the PE cylindrical domains are more isolated (i.e., there is less interconnection) in the morphology generated in the PS-*b*-PE-*b*-PEO sequence than in PE-*b*-PS-*b*-PEO.

(Insert Figure 7)

The rate of crystallization of the PE block is illustrated in Figure 7b as $1/\tau_{10\%}$. This value is more reliable than $1/\tau_{50\%}$, since the experiments were carried out with the step

crystallization technique. The limitation of the technique is the large experimental time and consequently there are only few measurements at times close to 50% of crystallization, compared to the measurements during the initial stages. The calculated errors have been included for the sake of clarity. The crystallization rate decreases when the block sequence is changed from the end to the middle, clearly due to the loss of mobility by chain tethering at both ends. This effect has been reported previously by Weimann et al.,[45] who found that larger supercooling was required for crystallization of the polyethylene block in polyvinylcyclohexane-*block*-polyethylene-*block*-polyvinylcyclohexane than in polyethylene-*block*-polyvinylcyclohexane .

It is worth noting that, the decrease in crystallization rate when going from a lamellar morphology ($E_{38}S_{16}EO_{46}^{77}$) to a cylindrical one ($E_{29}S_{40}EO_{31}^{170}$) is much higher than the decrease observed due to alternation in block sequence (Figure 7). This result could indicate that the confinement of the crystallization in a microphase with higher interfacial area implies not only a decrease of chain mobility and diffusion, but one might speculate that it also implies a decrease in nucleation rate (since heterogeneous nucleation is less probable as MD size decreases).[5]

Self-nucleation experiments. In order to study the crystallization within the terpolymer with the lowest content of crystallizable blocks, self-nucleation experiments were done on $B_{16}S_{68}EO_{16}^{210}$ and $E_{17}S_{67}EO_{16}^{211}$. The aim of the experiments was to determine whether the crystallization is totally confined inside the spherical microphases. This is achieved by subjecting the sample to a thermal protocol where it is forced to crystallize from homogeneous nuclei. The nuclei consist of unmolten polymer crystals generated under standardized conditions, as described in the experimental section. Figures 8 and 9 show the cooling and heating scans for the PEO block in the non-hydrogenated and the hydrogenated triblock terpolymers, respectively. Studies were also performed on the PE block, and the

cooling scans and subsequent heating scans are presented in Figure 10. In Figure 11 the domain definitions are presented for both terpolymers.

In both cooling DSC scans presented in Figures 8a and 9a the exotherms that appear at very low temperatures (peak crystallization temperatures of approximately -20 °C and -30 °C respectively) are due to the crystallization of confined PEO spheres. It is now well known that when a polymer is confined in a large number of microphase domains (MD), and if the density of MD is much larger than the available heterogeneities in the system, the nucleation mechanism changes from heterogeneous to superficial and/or homogeneous.[5, 13]

In the cooling scans presented in Figure 8a for $B_{16}S_{68}EO_{16}$[210], the crystallization peaks observed in the standard scan (T_s = 100 °C) showed no shifts to higher temperatures for T_s > 60 °C. This indicates that no self-nucleation occurs at higher temperatures. The heating scans presented in Figure 8b show the appearance of a high temperature melting signal at T_s = 64 °C, corresponding to the crystals annealed at T_s. This temperature marks the transition from Domain I to Domain III_A, a domain of exclusive annealing where no self-nucleation takes place. Self-nucleation is detected at 60 °C as indicated by the decrease in the crystallization peak temperature. This corresponds to the transition to Domain III_{SA}, where both self-nucleation and annealing take place. Since there is no T_s found where only self-nucleation occurs, the Domain II is absent. This behavior is commonly assigned to a crystallization induced by simultaneous nucleation at the interfaces instead of sporadic nucleation from heterogeneities.[5]

(Insert Figure 8)

The results of the self-nucleation studies for the PEO block in the hydrogenated terpolymer, $E_{17}S_{67}EO_{16}$[211] (Figure 9), demonstrate no major variations after hydrogenation. Since no shift was observed in the crystallization peak temperature signal, there is no domain where self-

nucleation takes place (Domain II or Domain III_{SA}). The annealing of the crystals is evident at T_s = 58 °C, which is the transition from Domain I or complete melting domain to Domain III_A or annealing domain. As in the non-hydrogenated triblock terpolymer case, the absence of Domain II or self-nucleation domain is evident.

(Insert Figure 9)

The study of the self-nucleation behavior of the PE block in $E_{17}S_{67}EO_{16}$[211] is presented in Figure 10. Similar to the case of the PEO block in the same triblock terpolymer, no shift was observed in the crystallization temperature when T_s was decreased. Only the annealing of the crystals could be evidenced, as indicated by the arrow in Figure 10b, at T_s = 96 °C. These and the previously discussed results are summarized in Figure 11. For all the studied cases, transitions from Domain I to Domain III_A where observed. The absence of the self-nucleation domain (Domain II) indicates instantaneous nucleation, which usually is a sign that the crystallization occurs confined within the microphases.[9,16] Based on the morphology determination it can be assumed that isolated PEO or PE/PEO spheres are distributed in the PS matrix and crystallization occurs (almost) exclusively inside them. These results are consistent with the crystallization kinetics results, corresponding to a first order kinetics, i.e., Avrami indices close to 1, as was observed in Figure 2a.

(Insert Figure 10)

(Insert Figure 11)

Conclusion

Due to the wide compositional range and variety of triblock terpolymers in this work, the crystallization kinetics of PEO and PE blocks has been studied as a function of mainly two parameters: microphase geometry and microphase surroundings. For the case of the

microphase geometry, it was found that the crystallization rate decreases with the block content, i.e., from interconnected lamellae or cylinders to isolated spheres. The relative crystallinity as a function of time showed a sigmoidal shape for lamellae and cylinders, and the calculated Avrami indices had values typical for conventional spherulitic crystallization from heterogeneities. First order nucleation controlled kinetics was found for the PEO spheres. These results were consistent with the self-nucleation experiments carried out, where the Domain II (self-nucleation domain) was absent for all sphere forming blocks.

The surroundings were analyzed elaborating different comparisons. It was found that a second crystalline PE end block increases the crystallization rate of the PEO block, with respect to a amorphous PB end block. This was attributed to the overcoming of the activation energy barrier of nucleation, assisted by the chain stretching caused by PE crystallization. However, if the PE block is a direct neighbor of the PEO block, the crystallization rate decreases slightly due to its anchoring effect. The crystallization rate decreases in soft confinements, which is attributed to a decrease in the segmental alignment to the nuclei caused by the high mobility of the rubbery neighbor block.

The crystallization kinetics of the PE block revealed a high importance of the microphase geometry. The lowest crystallization rate was found when the PE was the middle block and formed cylinders, which also followed a first order crystallization kinetics. A higher rate was observed for PE end blocks forming cylinders, and a remarkably higher rate was shown for the lamellae forming PE at the end block position. Restricting the microphase geometry decreased the crystallization rate more than mobility restrictions given by chain tethering at both ends. This implies that the restrictions of the microdomain geometry do not only limit the diffusion phase of crystallization to a higher extend but also affect the nucleation stage of crystallization, since the probability of heterogeneous nucleation decreases with an increase in MD density.

Appendices

The morphology of the of $S_{43}E_{22}EO_{35}^{112}$ triblock terpolymer was observed by transmission electron microscopy of a ultrathin cut of a film cast from a toluene solution. The micrograph is presented in Figure A, where the cylindrical morphology can be appreciated.

(Insert Figure A)

Acknowledgments

The contributions of Mariselis Trujillo (Universidad Simón Bolívar) and Julio Albuerne (GKSS Research Centre Geesthacht GmbH) are acknowledged. This work was partially supported by Deutsche Forschungsgemeinschaft and the European Action COST P12.

References

[1] [1a] I. W. Hamley, "*The Physics of Block Copolymers*", 1st edition, Oxford University Press, Oxford 1998, p. 432; [1b] H.-L. Chen, S.-C. Hsiao, T.-L. Lin, K. Yamauchi, H. Hasegawa, T. Hashimoto, *Macromolecules* **2001,** *34*, 671; [1c] L. Li, Y. Serero, M. H. J. Koch, W. H. de Jeu, *Macromolecules* **2003,** *36*, 529.

[2] L. Zhu, H.-L. Chen, B. H. Calhoun, Q. Ge, R. P. Quirk, E. L. Thomas, B. S. Hsiao, F. Yeh, B. Lotz, *Polymer* **2001,** *42*, 5829.

[3] H. Schmalz, A. J. Müller, V. Abetz, *Macromol. Chem. Phys.* **2003,** *204*, 111.

[4] L. Sun, Y. Lui, L. Zhu, B. S. Hsiao, C. A. Avila-Orta, *Polymer* **2004,** *2004*, 8181.

[5] A. J. Müller, V. Balsamo, M. L. Arnal, *Adv. Polym. Sci.* **2005,** *190*, 1.

[6] H. Schmalz, A. Böker, R. Lange, G. Krausch, V. Abetz, *Macromolecules* **2001,** *34*, 8720.

[7] V. Balsamo, N. Urdaneta, L. Pérez, P. Carrizales, V. Abetz, A. J. Müller, *Eur. Polym. J.* **2004,** *40*, 1033.

[8] A. J. Müller, V. Balsamo, M. L. Arnal, in: *Lecture Notes in Physics: Progress in Understanding of Polymer Crystallization*, G. Reiter, G. Strobl, Eds., Springer, Berlin 2007, pp 229.

[9] [9a] I. W. Hamley, J. P. A. Fairclough, F. S. Bates, A. J. Ryan, *Polymer* **1998,** *39*, 1429; [9b] Y.-L. Loo, R. A. Register, "Crystallization within block copolymer mesophases", in: *Development in block copolymer science and technology*, I. W. Hamley, Ed. John Wiley & Sons, Ltd, 2004, pp 213.

[10] [10a] A. J. Ryan, I. W. Hamley, W. Bras, F. S. Bates, *Macromolecules* **1995,** *28*,

3860; [10b] I. W. Hamley, *Adv. Polym. Sci.* **1999,** *148*, 113; [10c] G. Floudas, B. Vazaiou, F. Schipper, R. Ulrich, U. Wiesner, H. Iatrou, N. Hadjichristidis, *Macromolecules* **2001,** *34*, 2947.

[11] Y.-L. Loo, R. A. Register, A. J. Ryan, G. T. Dee, *Macromolecules* **2001,** *34*, 8968.

[12] Y.-L. Loo, R. A. Register, A. J. Ryan, *Macromolecules* **2002,** *35*, 2365.

[13] A. J. Müller, V. Balsamo, M. L. Arnal, T. Jakob, H. Schmalz, V. Abetz, *Macromolecules* **2002,** *35*, 3048.

[14] P. Rangarajan, R. A. Register, D. H. Adamson, L. J. Fetters, W. Bras, S. Naylor, A. J. Ryan, *Macromolecules* **1995,** *28*, 1422.

[15] F. S. F. Bates, Glenn H., *Phys. Today* **1999,** *52*, 32.

[16] [16a] R. E. Cohen, P.-L. Cheng, K. Douzinas, P. Kofinas, C. V. Berney, *Macromolecules* **1990,** *23*, 324; [16b] R. Séguéla, J. Prud'homme, *Polymer* **1989,** *30*, 1446.

[17] [17a] L. Sun, L. Zhu, Q. Ge, R. P. Quirk, C. Xue, S. Z. D. Cheng, B. S. Hsiao, C. A. Avila-Orta, I. Sics, M. E. Cantino, *Polymer* **2004,** *45*, 2931; [17b] L. Zhu, S. Z. D. Cheng, P. Huang, Q. Ge, R. P. Quirk, E. L. Thomas, B. Lotz, B. S. Hsiao, F. Yeh, L. Liu, *Adv. Mater.* **2002,** *14*, 31; [17c] L. Zhu, B. R. Mimnaugh, Q. Ge, R. P. Quirk, S. Z. D. Cheng, E. L. Thomas, B. Lotz, B. S. Hsiao, F. Yeh, L. Liu, *Polymer* **2001,** *42*, 9121.

[18] [18a] B. Heck, T. Hugel, M. Iijima, G. Strobl, *Polymer* **2000,** *41*, 8839; [18b] G. Strobl, *Eur. Phys. J. E* **2000,** *V3*, 165; [18c] M. Muthukumar, P. Welch, *Polymer* **2000,** *41*, 8833; [18d] M. Muthukumar, *Eur. Phys. J. E* **2000,** *3*, 199.

[19] H. Schmalz, V. Abetz, R. Lange, M. Soliman, *Macromolecules* **2001,** *34*, 795.

[20] [20a] B. Esswein, A. Molenberg, M. Möller, *Macromol. Symp.* **1996,** *107*; [20b] B. Esswein, M. Möller, *Angew. Chem.* **1996,** *108*, 703; [20c] B. Esswein, N. M. Steidl, M. Möller, *Macromol. Rapid Commun.* **1996,** *17*, 143; [20d] G. Floudas, B. Vazaiou, F. Schipper, R. Ulrich, U. Wiesner, H. Iatrou, N. Hadjichristidis, *Macromolecules* **2001,** *34*, 2947; [20e] S. Förster, E. Krämer, *Macromolecules* **1999,** *32*, 2783.

[21] M. J. Galante, L. Mandelkern, R. G. Alamo, A. Lehtinen, R. Paukkeri, *J. Therm. Anal. Calorim.* **1996,** *47*, 913.

[22] B. Fillon, J. C. Wittmann, B. Lotz, A. Thierry, *J. Polym. Sci. B: Polym. Phys.* **1993,** *31*, 1383.

[23] A. Boschetti-de-Fierro, A. J. Müller, V. Abetz, *Macromolecules* **2007,** *40*, 1290.

[24] A. T. Lorenzo, M. L. Arnal, J. Albuerne, A. J. Müller, *Polym. Test.* **2007,** *26*, 222.

[25] [25a] M. Avrami, *J. Chem. Phys.* **1939,** *7*, 1103; [25b] *J. Chem. Phys.* **1940,** *8*, 212.

[26] M. Avrami, *J. Chem. Phys.* **1941,** *9*, 177.

[27] E. Piorkowska, A. Galeski, J.-M. Haudin, *Prog. Polym. Sci.* **2006,** *31*, 549.

[28] [28a] A. J. Müller, J. Albuerne, L. M. Esteves, L. Marquez, J.-M. Raquez, P. Degée, P. Dubois, S. Collins, I. W. Hamley, *Macromol. Symp.* **2004,** *215*, 369; [28b] H.-L. Chen, S.-Y. Lin, Y.-Y. Huang, F.-C. Chiu, W. Liou, J. S. Lin, *Macromolecules* **2002,** *35*, 9434; [28c] I. W. Hamley, V. Castelletto, R. V. Castillo, A. J. Müller, C. M. Martin, E. Pollet, P. Dubois, *Macromolecules* **2005,** *38*, 463; [28d] U. Jeong, H. H. Lee, H. Yang, J. K. Kim, S. Okamoto, S. Aida, S. Sakurai, *Macromolecules* **2003,** *36*, 1685; [28e] L. Sun, L. Zhu, Q. Ge, R. P. Quirk, C. Xue, S. Z. D. Cheng, B. S. Hsiao, C. A. Avila-Orta, I. Sics, M. E. Cantino, *Polymer* **2004,** *45*, 2931; [28f] G. Floudas, C. Tsitsilianis, *Macromolecules* **1997,** *30*, 4381; [28g] I. Alig, S. Tadjbakhsch, G. Floudas, C. Tsitsilianis, *Macromolecules* **1998,** *31*, 6917; [28h] H.

Takeshita, N. Ishii, C. Araki, M. Miya, K. Takenaka, T. Shiomi, *J. Polym. Sci. B: Polym. Phys.* **2004,** *42*, 4199; [28i] I. W. Hamley, P. Parras, V. Castelletto, R. V. Castillo, A. J. Müller, E. Pollet, P. Dubois, C. M. Martin, *Macromol. Chem. Phys.* **2006,** *207*, 941.

[29] J. Albuerne, L. Márquez, A. J. Müller, J. M. Raquez, P. Degée, P. Dubois, V. Castelletto, I. W. Hamley, *Macromolecules* **2003,** *36*, 1633.

[30] H.-L. Chen, J.-C. Wu, T.-L. Lin, J. S. Lin, *Macromolecules* **2001,** *34*, 6936.

[31] R.-M. Ho, Y.-W. Chiang, C.-C. Lin, B.-H. Huang, *Macromolecules* **2005,** *38*, 4769.

[32] T. Shiomi, H. Takeshita, H. Kawaguchi, M. Nagai, K. Takenaka, M. Miya, *Macromolecules* **2002,** *35*, 8056.

[33] [33a] E. Piorkowska, A. Galeski, *J. Phys. Chem.* **1985,** *89*, 4700; [33b] *J. Appl. Polym. Sci.* **2002,** *86*, 1363; [33c] *J. Macromol. Sci. Part B-Phys.* **2003,** *42*, 773.

[34] Y.-L. Loo, R. A. Register, A. J. Ryan, *Phys. Rev. Lett.* **2000,** *84*, 4120 LP

[35] [35a] D. Turnbull, R. L. Cormia, *J. Chem. Phys.* **1961,** *34*, 820; [35b] R. L. Cormia, F. P. Price, D. Turnbull, *J. Chem. Phys.* **1962,** *37*, 1333.

[36] A. Boschetti-de-Fierro, L. Spindler, G. Reiter, D. Olmos, S. Magonov, V. Abetz, *Macromolecules* **2007,** *40*, 5487.

[37] R. Opitz, D. M. Lambreva, W. H. de Jeu, *Macromolecules* **2002,** *35*, 6930.

[38] X. Zhang, Z. Wang, X. Dong, D. Wang, C. C. Han, *J. Chem. Phys.* **2006,** *125*, 024907.

[39] H. Schmalz, A. Knoll, A. J. Müller, V. Abetz, *Macromolecules* **2002,** *35*, 10004.

[40] A. J. Müller, J. Albuerne, L. Márquez, J.-M. Raquez, P. Degée, P. Dubois, J. Hobbs, I. W. Hamley, *Faraday Discuss.* **2005,** *128*, 231.

[41] M. Ueda, K. Sakurai, S. Okamoto, D. J. Lohse, W. J. MacKnight, S. Shinkai, S. Sakurai, S. Nomura, *Polymer* **2003,** *44*, 6995.

[42] T. H. Epps, T. S. Bailey, R. Waletzko, F. S. Bates, *Macromolecules* **2003,** *36*, 2873.

[43] A. J. Müller, A. T. Lorenzo, R. V. Castillo, M. L. Arnal, A. Boschetti-de-Fierro, V. Abetz, *Macromol. Symp.* **2006,** *245/246*, 154.

[44] A. T. Lorenzo, M. L. Arnal, A. J. Müller, A. Boschetti-de-Fierro, V. Abetz, *Macromolecules* **2007,** *40*, 5023.

[45] P. A. Weimann, D. A. Hajduk, C. Chu, K. A. Chaffin, J. C. Brodil, F. S. Bates, *J. Polym. Sci. B: Polym. Phys.* **1999,** *37*, 2045.

[46] A. Boschetti-de-Fierro, D. Fierro, J. Albuerne, S. S. Funari, V. Abetz, *J. Polym. Sci. B: Polym. Phys.* **2007,** *submitted*.

Captions to Figures/Schemes:

Figure 1. (a) DSC isothermal scans for $B_{29}S_{40}EO_{31}^{168}$ at different crystallization temperatures. (b) Relative crystallinity, calculated from the isothermal scans in (a), as a function of the crystallization time for the different crystallization temperatures employed.

Figure 2. Crystallization kinetics for the PEO block in triblock terpolymers with different compositions: □ $B_{16}S_{68}EO_{16}^{210}$, △ $B_{29}S_{40}EO_{31}^{168}$ and ○ $B_{37}S_{16}EO_{47}^{76}$. (a) Development of the relative crystallinity with time during isothermal crystallization at 48.0 °C (40 °C for $B_{16}S_{68}EO_{16}^{210}$). (b) Inverse of experimental crystallization half-time as a function of crystallization temperature.

Figure 3. Crystallization kinetics for the PEO block in triblock terpolymers before and after hydrogenation of the PB block. (a) Development of the relative crystallinity with time during isothermal crystallization at 49.5 °C. (b) Inverse of experimental crystallization half-time as a function of crystallization temperature: △ $B_{29}S_{40}EO_{31}^{168}$ and □ $E_{29}S_{40}EO_{31}^{170}$.

Figure 4. Crystallization kinetics for the PEO block in triblock terpolymers with similar compositions but different block sequence. (a) Development of the relative crystallinity with time during isothermal crystallization at 52.5 °C. (b) Inverse of experimental crystallization half-time as a function of crystallization temperature: △ $E_{16}S_{40}EO_{44}^{144}$ and □ $S_{43}E_{22}EO_{35}^{112}$.

Figure 5. Crystallization kinetics for the PEO block in triblock terpolymers with similar compositions but different middle block. (a) Development of the relative crystallinity with time during isothermal crystallization at 52.0 °C. (b) Inverse of experimental crystallization half-time as a function of crystallization temperature: △ $E_{16}S_{40}EO_{44}^{143}$ and □ $E_{19}EP_{40}EO_{41}^{138}$.

Figure 6. Crystallization kinetics for the PEO block in triblock terpolymers with similar compositions but different block sequence. (a) Development of the relative crystallinity with time during isothermal crystallization at 50.5 °C for $B_{16}S_{40}EO_{44}^{143}$ and 47.0 °C for $S_{43}B_{21}EO_{36}^{111}$. (b) Inverse of experimental crystallization half-time as a function of crystallization temperature: △ $B_{16}S_{40}EO_{44}^{143}$ and □ $S_{43}B_{21}EO_{36}^{111}$.

Figure 7. Crystallization kinetics for the PE block in triblock terpolymers with different compositions and block sequence: △ $E_{29}S_{40}EO_{31}^{170}$, ○ $E_{38}S_{16}EO_{46}^{77}$, and □ $S_{43}E_{22}EO_{35}^{112}$. (a) Development of the relative crystallinity with time during isothermal crystallization at 73.0 °C (80.0 °C for $E_{38}S_{16}EO_{46}^{77}$). (b) Inverse of experimental time at 10% of crystallization ($\tau_{10\%,\,exp.}$) as a function of crystallization temperature.

Figure 8. Self-nucleation experiments of the PEO block in $B_{16}S_{68}EO_{16}^{210}$: (a) cooling scans at 10 °C/min after 5 min at indicated T_s, (b) subsequent heating scans at 10 °C/min. Arrows indicate: (a) shift of crystallization peak to lower temperature, and (b) melting peak of annealed crystals.

Figure 9. Self-nucleation experiments of the PEO block in $E_{17}S_{67}EO_{16}^{211}$: (a) cooling scans at 10 °C/min after 5 min at indicated T_s, (b) subsequent heating scans at 10 °C/min. Arrow indicates melting peak of annealed crystals.

Figure 10. Self-nucleation experiments of the PE block in $E_{17}S_{67}EO_{16}^{211}$: a) cooling scans at 10 °C/min after 5 min at indicated T_s, b) subsequent heating scans at 10 °C/min. Arrow indicates melting peak of annealed crystals.

Figure 11. Definition of self-nucleation domains for PE and PEO blocks in (a) $B_{16}S_{68}EO_{16}^{210}$ and (b) $E_{17}S_{67}EO_{16}^{211}$, represented on the heating scan at 10 °C/min.

Figure A. TEM micrograph and morphology sketch for $S_{43}E_{22}EO_{35}^{112}$. Sketch color assignment: PS dark gray, PE light gray, PEO white. Ultrathin sections were obtained from films cast from toluene solutions at 70 °C, and stained with RuO_4 vapor.

Tables:

Table 1. Molecular weight of the blocks, molecular weight distributions of the overall terpolymer and content of 1,2 units in the polybutadiene block, for the terpolymers synthesized.

Terpolymer	M_n (Kg/mol)			M_w/M_n [a)]
	PB[a] (%1,2[b)]) / PE[c)]	PS[c)]	PEO[c)]	
$B_{29}S_{40}EO_{31}^{168}$ / $E_{29}S_{40}EO_{31}^{170}$	48 (12.9) / 50	67	53	1.03
$B_{17}S_{68}EO_{16}^{210}$ / $E_{17}S_{67}EO_{16}^{211}$	35 (11.5) / 36	142	33	1.01
$B_{16}S_{40}EO_{44}^{143}$ / $E_{16}S_{40}EO_{44}^{144}$	22 (14.0) / 23	58	63	1.05
$B_{37}S_{16}EO_{47}^{76}$ / $E_{38}S_{16}EO_{46}^{77}$	28 (11.8) / 29	13	36	1.03
$S_{30}B_{22}EO_{48}^{98}$ / $S_{30}E_{23}EO_{47}^{99}$	22 (11.1) / 23	29.5	47	1.01

[a)] Determined by SEC in THF calibrated against PB standards. [b)] Determined by ^{1}H NMR spectroscopy in $CDCl_3$. [c)] Determined by ^{1}H NMR spectroscopy using the molecular weight of the PB precursor obtained by SEC.

Table 2. Morphologies of the triblock terpolymers, as determined by TEM micrographs and SAXS patterns.

Terpolymer	TEM	SAXS
$B_{29}S_{40}EO_{31}^{168}$ / $E_{29}S_{40}EO_{31}^{170}$	Connected PEO cylinders	Hexagonally packed cylinders
$B_{16}S_{68}EO_{16}^{210}$ / $E_{17}S_{67}EO_{16}^{211}$	PEO and PB spheres / PEO and PE share spherical domains	*fcc*-packed spheres
$B_{16}S_{40}EO_{44}^{143}$ / $E_{16}S_{40}EO_{44}^{144}$	Lamellae / Poorly defined	Lamellae / Hexagonally packed cylinders
$B_{37}S_{16}EO_{47}^{76}$ / $E_{38}S_{16}EO_{46}^{77}$	Lamellae	Lamellae
$S_{43}B_{21}EO_{36}^{111}$ / $S_{43}E_{22}EO_{35}^{112}$,[a)]	PEO lamellae, PE cylinders	-

[a)] The results for these triblock terpolymers were not presented in ref. 23 or 46. The TEM micrograph of $S_{43}E_{22}EO_{35}^{112}$ is available in the appendices section.

Figures:

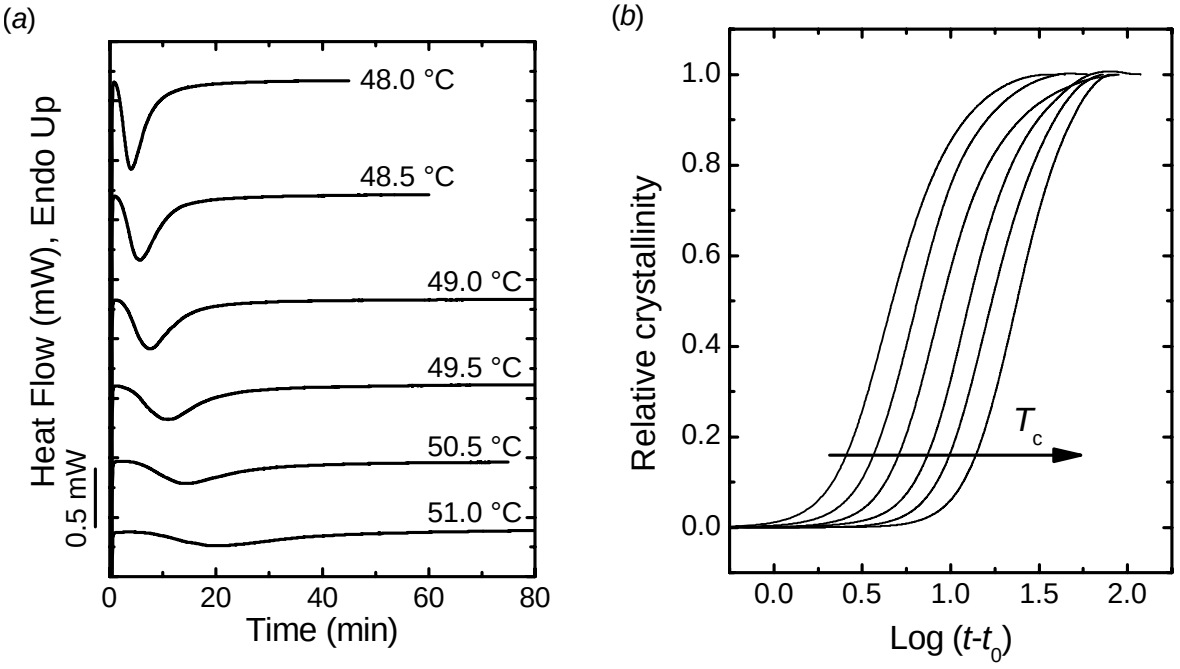

Figure 1. (a) DSC isothermal scans for $B_{29}S_{40}EO_{31}^{168}$ at different crystallization temperatures. (b) Relative crystallinity, calculated from the isothermal scans in (a), as a function of the crystallization time for the different crystallization temperatures employed.

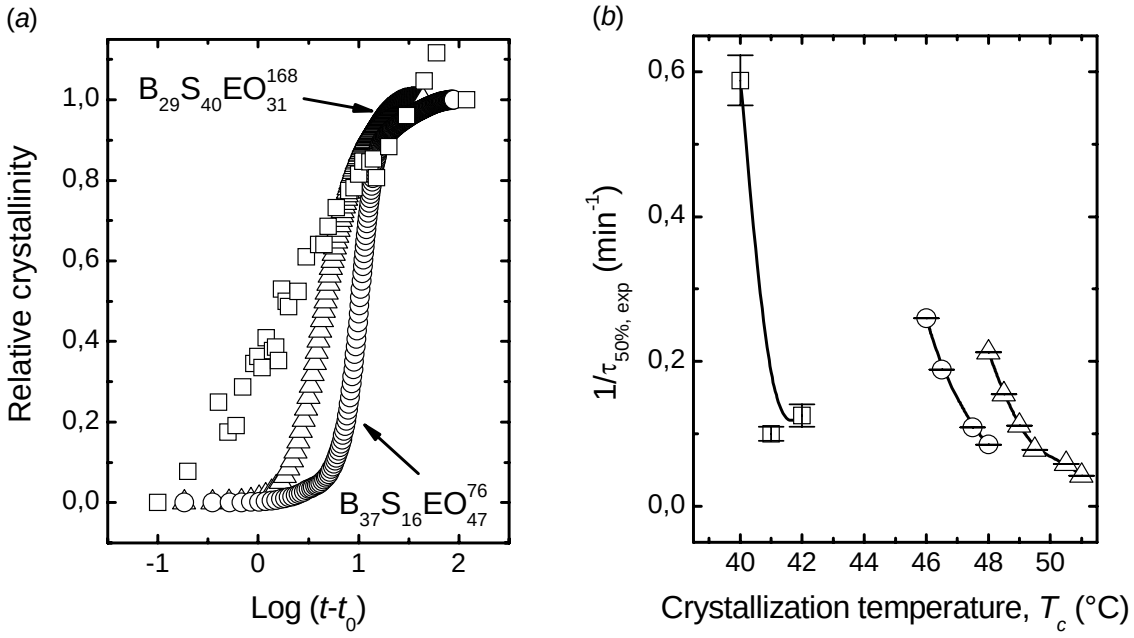

Figure 2. Crystallization kinetics for the PEO block in triblock terpolymers with different compositions: □ $B_{16}S_{68}EO_{16}^{210}$, △ $B_{29}S_{40}EO_{31}^{168}$ and ○ $B_{37}S_{16}EO_{47}^{76}$. (a) Development of the relative crystallinity with time during isothermal crystallization at 48.0 °C (40 °C for $B_{16}S_{68}EO_{16}^{210}$). (b) Inverse of experimental crystallization half-time as a function of crystallization temperature.

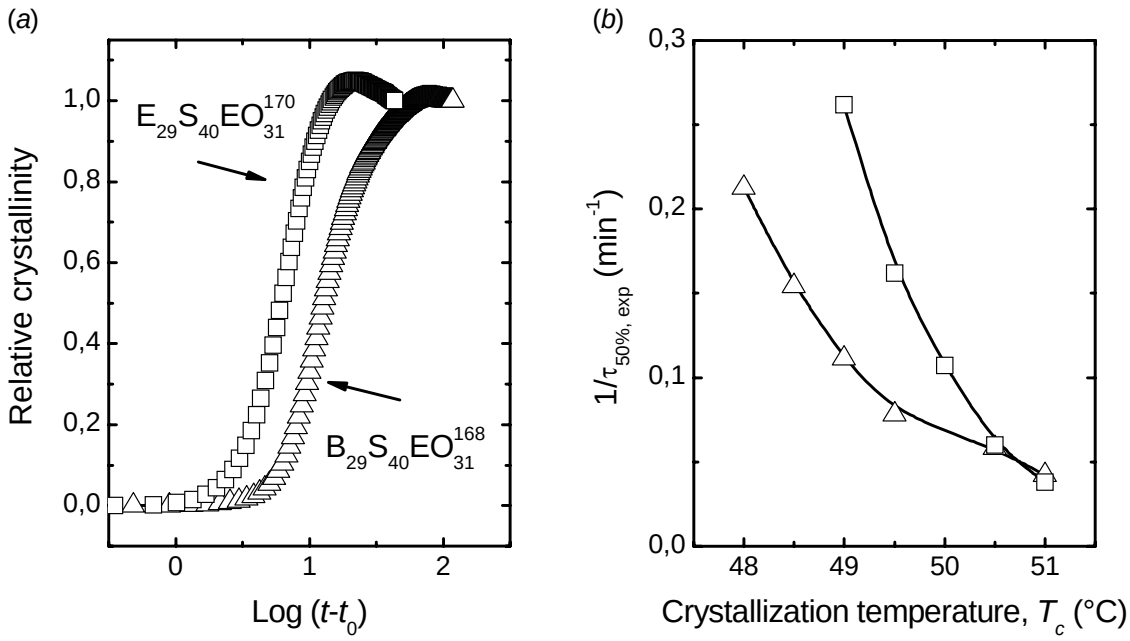

Figure 3. Crystallization kinetics for the PEO block in triblock terpolymers before and after hydrogenation of the PB block. (a) Development of the relative crystallinity with time during isothermal crystallization at 49.5 °C. (b) Inverse of experimental crystallization half-time as a function of crystallization temperature: △ $B_{29}S_{40}EO_{31}^{168}$ and □ $E_{29}S_{40}EO_{31}^{170}$.

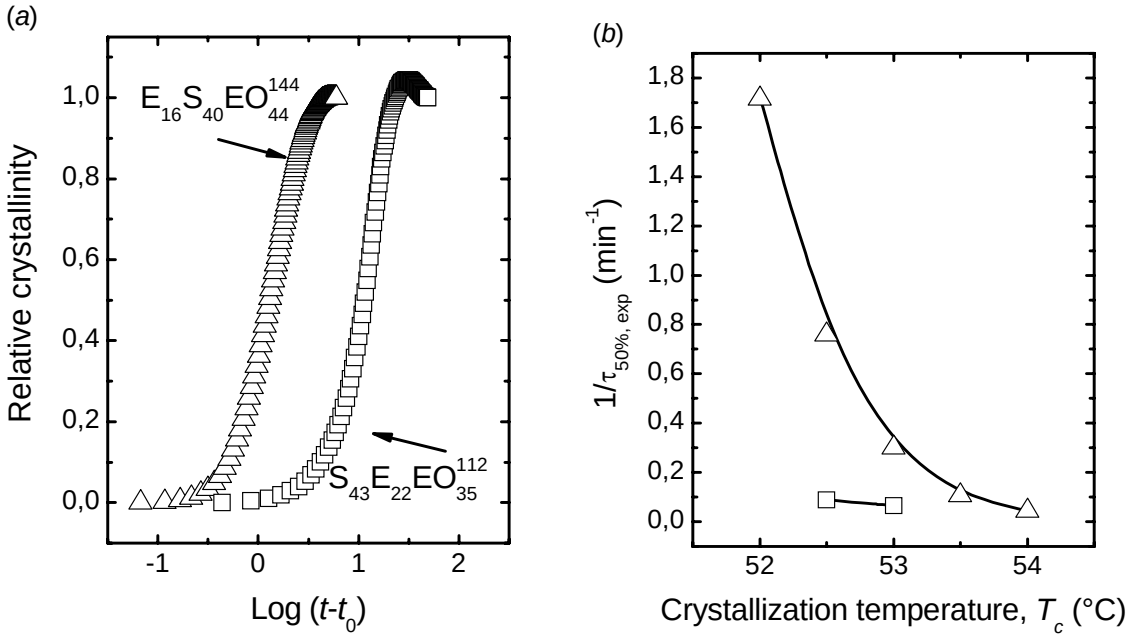

Figure 4. Crystallization kinetics for the PEO block in triblock terpolymers with similar compositions but different block sequence. (a) Development of the relative crystallinity with time during isothermal crystallization at 52.5 °C. (b) Inverse of experimental crystallization half-time as a function of crystallization temperature: △ $E_{16}S_{40}EO_{44}^{144}$ and □ $S_{43}E_{22}EO_{35}^{112}$.

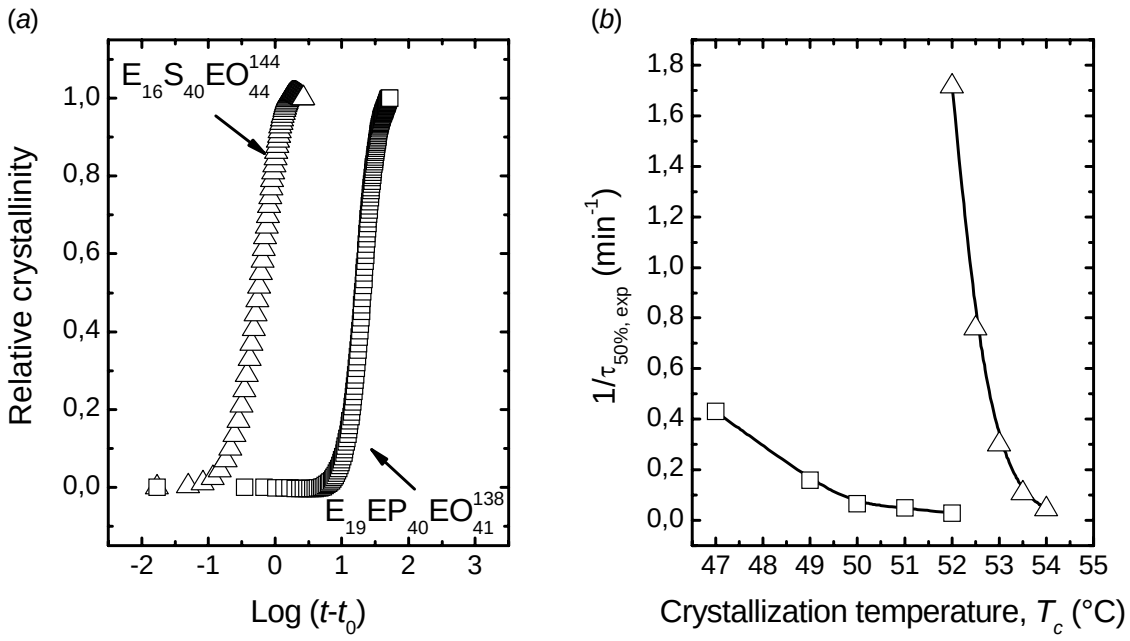

Figure 5. Crystallization kinetics for the PEO block in triblock terpolymers with similar compositions but different middle block. (a) Development of the relative crystallinity with time during isothermal crystallization at 52.0 °C. (b) Inverse of experimental crystallization half-time as a function of crystallization temperature: △ $E_{16}S_{40}EO_{44}$[143] and □ $E_{19}EP_{40}EO_{41}$[138].

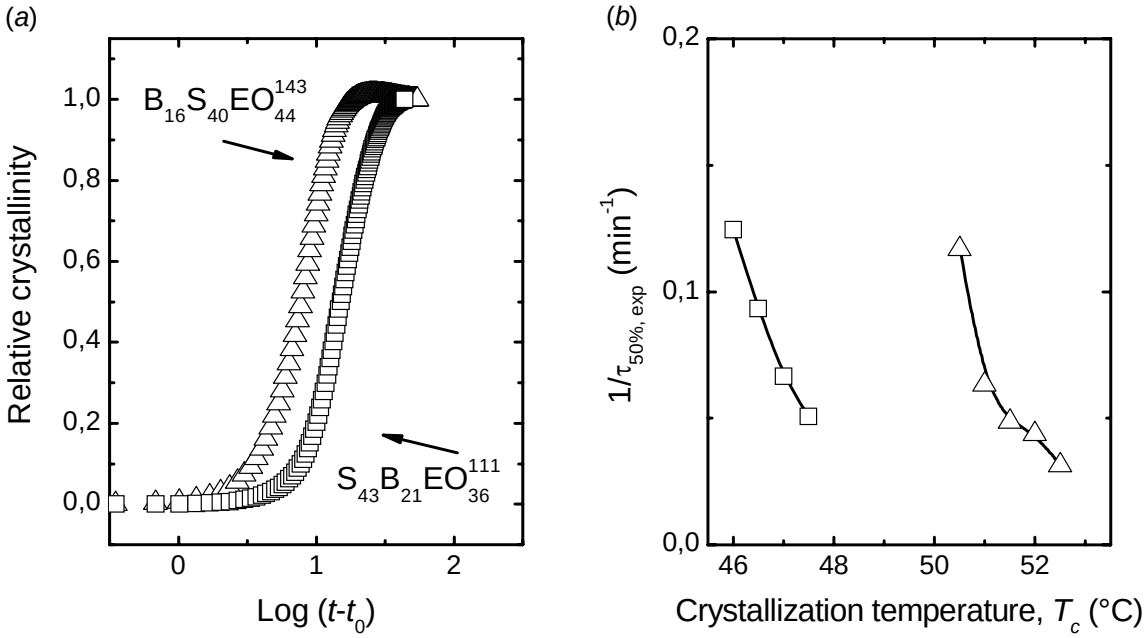

Figure 6. Crystallization kinetics for the PEO block in triblock terpolymers with similar compositions but different block sequence. (a) Development of the relative crystallinity with time during isothermal crystallization at 50.5 °C for $B_{16}S_{40}EO_{44}^{143}$ and 47.0 °C for $S_{43}B_{21}EO_{36}^{111}$. (b) Inverse of experimental crystallization half-time as a function of crystallization temperature: △ $B_{16}S_{40}EO_{44}^{143}$ and □ $S_{43}B_{21}EO_{36}^{111}$.

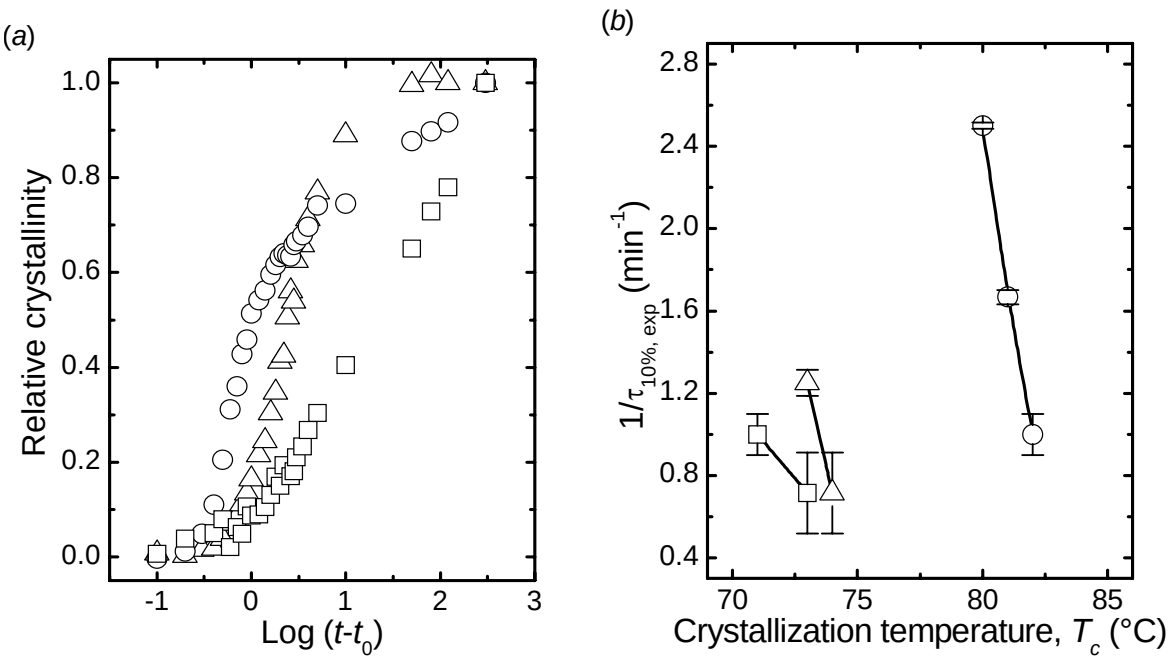

Figure 7. Crystallization kinetics for the PE block in triblock terpolymers with different compositions and block sequence: △ $E_{29}S_{40}EO_{31}^{170}$, ○ $E_{38}S_{16}EO_{46}^{77}$, and □ $S_{43}E_{22}EO_{35}^{112}$. (a) Development of the relative crystallinity with time during isothermal crystallization at 73.0 °C (80.0 °C for $E_{38}S_{16}EO_{46}^{77}$). (b) Inverse of experimental time at 10% of crystallization ($\tau_{10\%, exp.}$) as a function of crystallization temperature.

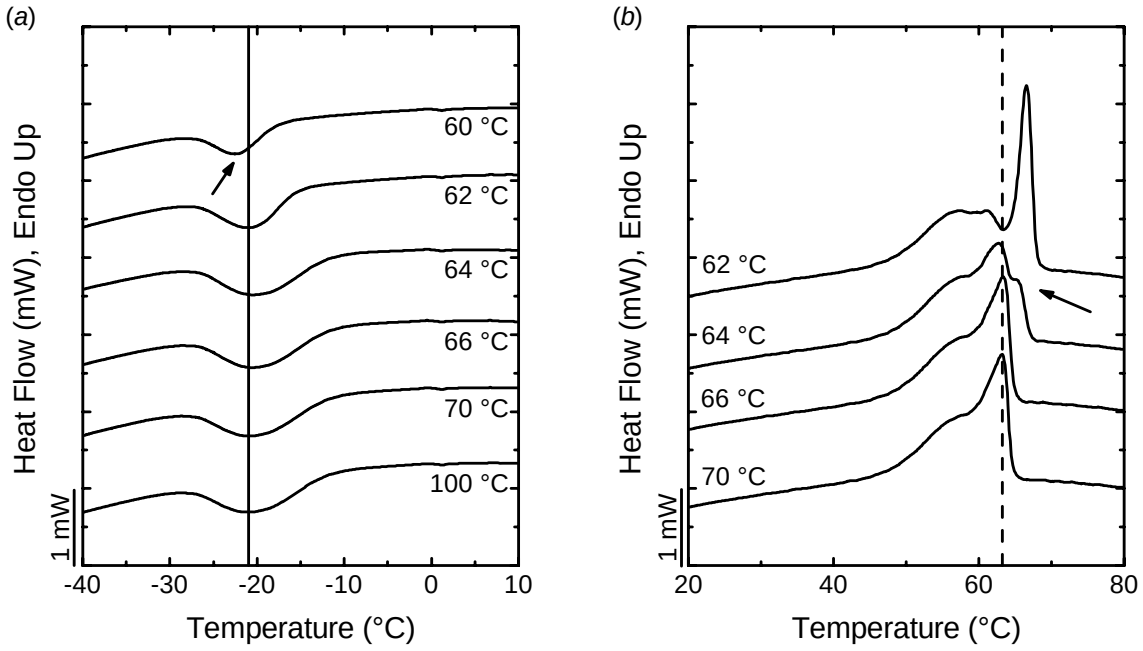

Figure 8. Self-nucleation experiments of the PEO block in $B_{16}S_{68}EO_{16}$[210]: (a) cooling scans at 10 °C/min after 5 min at indicated T_s, (b) subsequent heating scans at 10 °C/min. Arrows indicate: (a) shift of crystallization peak to lower temperature, and (b) melting peak of annealed crystals.

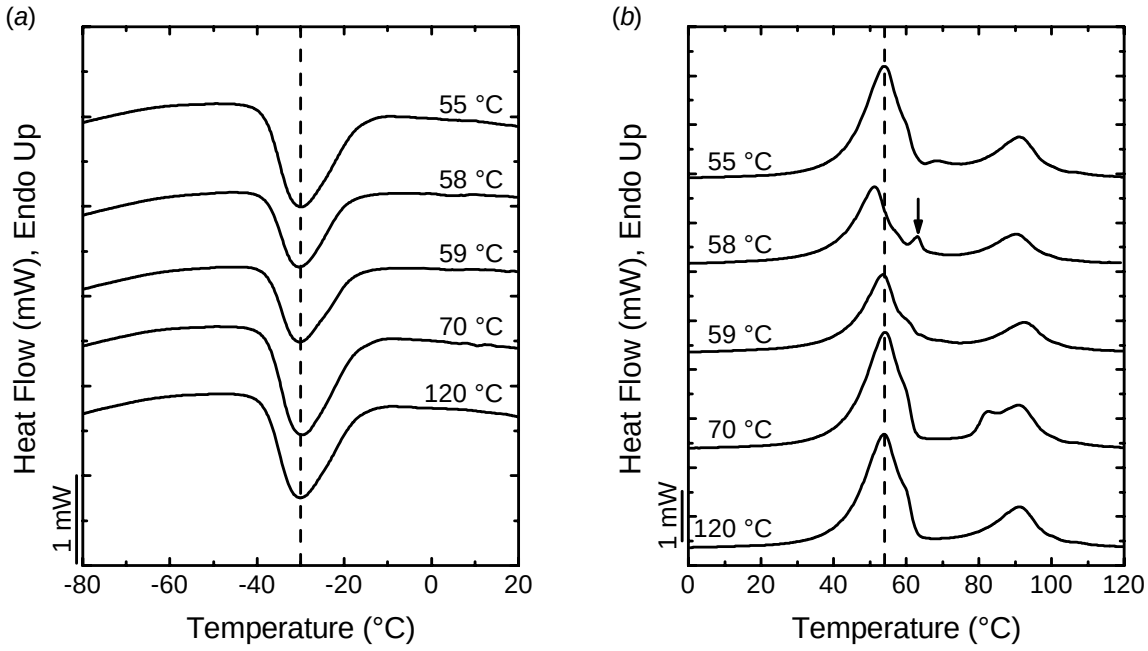

Figure 9. Self-nucleation experiments of the PEO block in $E_{17}S_{67}EO_{16}$[211]: (a) cooling scans at 10 °C/min after 5 min at indicated T_s, (b) subsequent heating scans at 10 °C/min. Arrow indicates melting peak of annealed crystals.

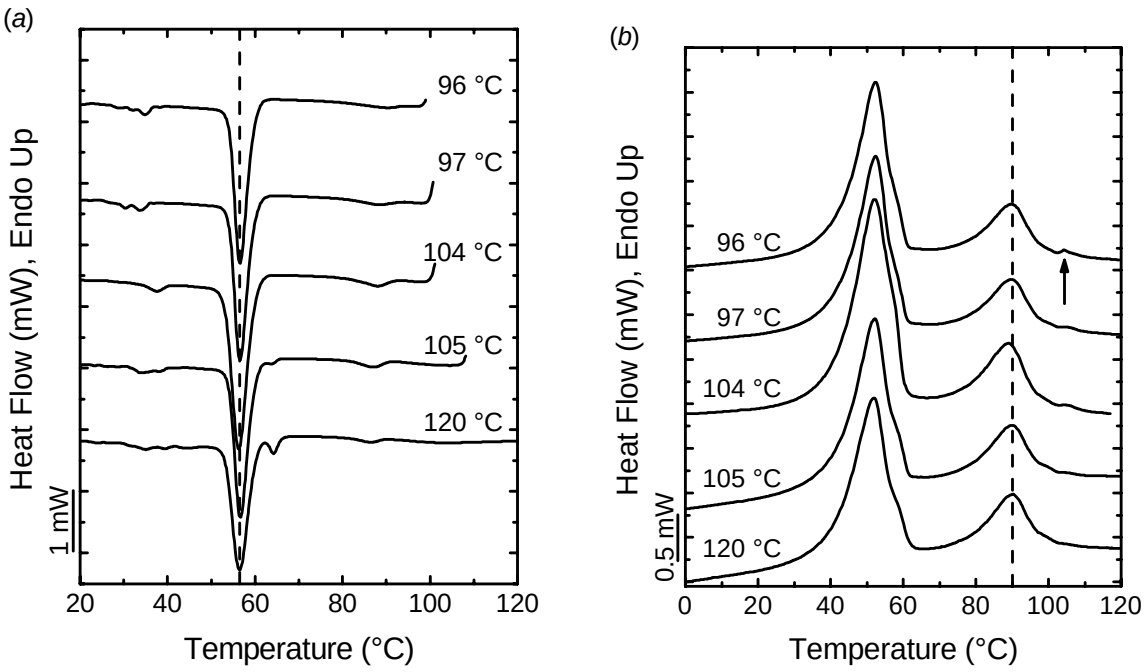

Figure 10. Self-nucleation experiments of the PE block in $E_{17}S_{67}EO_{16}$[211]: a) cooling scans at 10 °C/min after 5 min at indicated T_s, b) subsequent heating scans at 10 °C/min. Arrow indicates melting peak of annealed crystals.

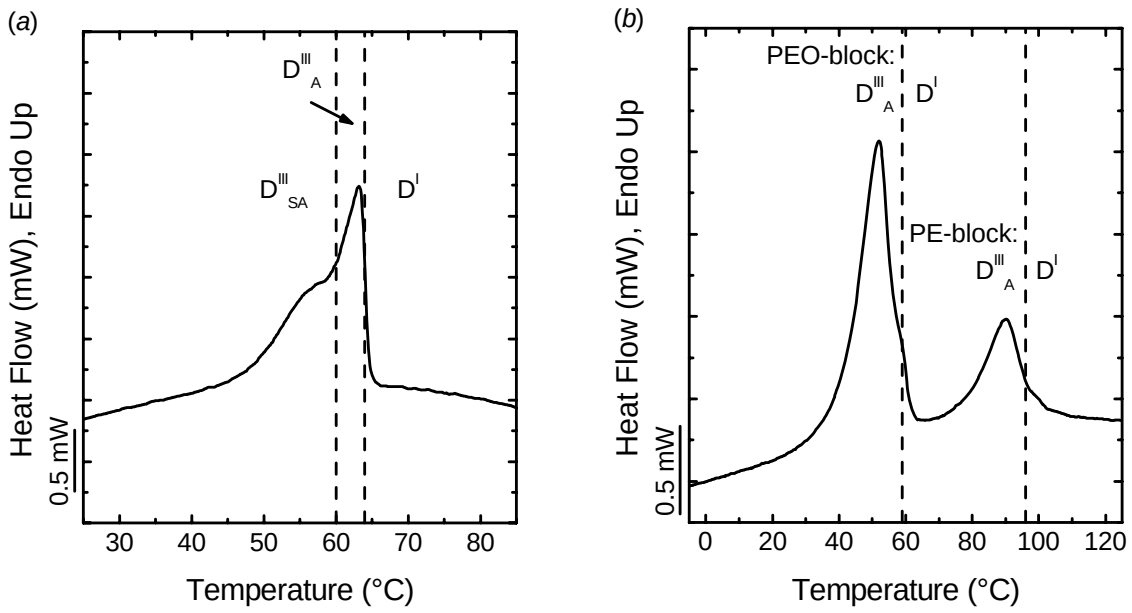

Figure 11. Definition of self-nucleation domains for PE and PEO blocks in (a) $B_{16}S_{68}EO_{16}$[210] and (b) $E_{17}S_{67}EO_{16}$[211], represented on the heating scan at 10 °C/min.

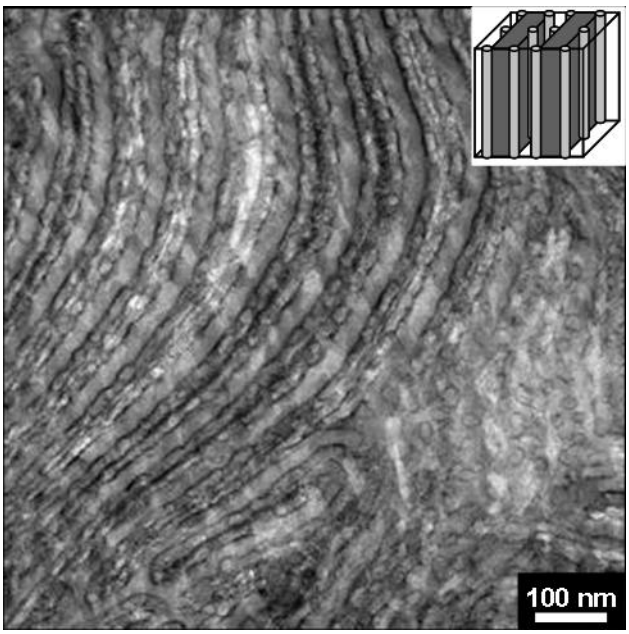

Figure A. TEM micrograph and morphology sketch for $S_{43}E_{22}EO_{35}$[112]. Sketch color assignment: PS dark gray, PE light gray, PEO white. Ultrathin sections were obtained from films cast from toluene solutions at 70 °C, and stained with RuO_4 vapor.

Text for Table of Contents:

Microdomains' geometry effect on the crystallization kinetics of PEO and PE in triblock terpolymers was analyzed for different compositions and block sequences of PB-*b*-PS-*b*-PEO and PE-*b*-PS-*b*-PEO. The crystallization curve shows the sigmoidal shape typical for homopolymers when the crystallization takes place in lamellae or cylinders, but it is exponential when it is confined to spheres. Crystallization rate decreases with the block content for both crystallizable blocks. PE crystallization induces chain stretching that aids the nucleation of PEO. Crystallization rate of PE decreases more strongly with the microdomain geometry reduction than by chain tethering.